Journal of Molecular Liquids 433 (2025) 127892

Contents lists available at ScienceDirect

Journal of Molecular Liquids

journal homepage: www.elsevier.com/locate/molliq

Dynamical processes and order behind the pronounced ^{1}H NMR paramagnetic relaxation enhancement induced in $[P_{6,6,6,14}]_3[GdCl_6]$-based ionic liquid mixtures

Maria J. Beira [a,b,*], Gonçalo M.C. Silva [c], Tiago M. Eusébio [c], João L. Figueirinhas [a], Rui Cordeiro [a], Carlos Cruz [a], Marta C. Corvo [d], Pedro L. Almeida [d,e], Andreia A. Rosatella [f,g], Carlos A.M. Afonso [f], Eduardo J.M. Filipe [c], Teodor Parella [h], Eurico J. Cabrita [i], Pedro J. Sebastião [a]

[a] Center of Physics and Engineering of Advanced Materials, Departamento de Física, Instituto Superior Técnico, Universidade de Lisboa, Av. António José de Almeida no. 12, 1000-043 Lisboa, Portugal
[b] HyLab - Green Hydrogen Collaborative Laboratory, Edifício da Quinta da Lameira, Sines Tecnopolo, ZIL II, Lote 122A, 7520-309 Sines, Portugal
[c] Centro de Química Estrutural, Departamento de Química, Instituto Superior Técnico, Universidade de Lisboa, Av. António José de Almeida no. 12, 1000-043 Lisboa, Portugal
[d] i3N|CENIMAT, Departamento de ciência dos Materiais, Nova School of Science and Technology, Campus de Caparica, 2829-516 Caparica, Portugal
[e] UnIRE and Mechanical Engineering Department, Instituto Superior de Engenharia de Lisboa (ISEL), 1959-007 Lisbon, Portugal
[f] Research Institute for Medicines (iMed.ULisboa), Faculty of Pharmacy, Universidade de Lisboa, Av. Prof. Gama Pinto, 1649-003 Lisboa, Portugal
[g] CBIOS - Research Center for Biosciences & Health Technologies, Universidade Lusófona, Campo Grande 376, 1749-024 Lisboa, Portugal
[h] Servei de RMN, Facultat de Ciències, Universitat Autònoma de Barcelona, Campus UAB, E-08193 Bellaterra, Catalonia, Spain
[i] UCIBIO, Departamento de Química, NOVA School of Science and Technology, Campus Caparica, 2829-516, Portugal

ARTICLE INFO

Keywords:
Magnetic ionic liquids
Local order fluctuations
^{1}H NMR relaxometry
Molecular dynamics simulations
Wide angle X-ray
EIS
Trihexyl(tetradecyl)phosphonium hexachlorogadolinium
Trihexyl(tetradecyl)phosphonium chloride

ABSTRACT

NMR relaxometry is a technique that allows the molecular dynamics study of chemical compounds across a broad time scale, ranging from slow translational diffusion or collective motions to fast rotations. The present work is a ^{1}H NMR relaxometry and diffusometry study of systems based on $[P_{6,6,6,14}][Cl]$ and $[P_{6,6,6,14}]_3[GdCl_6]$ ionic liquids, complemented by X-ray diffractometry measurements. The use of the X-ray profiles enabled the determination of an almost temperature independent interdigitated disposition of the cations that is at the origin of local order fluctuations. This structure also affects the paramagnetic relaxation enhancement, which is very significant for these systems and is achieved at very low metal concentrations (around 1mM). The present study provides a comprehensive analysis that is consistent for all the analyzed systems and across the different experimental techniques, despite the experienced technical challenges related to extremely short relaxation times. Additionally, the Electrochemical Impedance Spectroscopy profiles of the neat $[P_{6,6,6,14}][Cl]$ sample were explained by an analogous equivalent circuit model that allowed for a global analysis consistent with the diffusometry and X-ray diffractometry results. The representation of the real and imaginary parts of the impedance allowed for a visual deconvolution of the contributions of the different circuit blocks considered in the model.

1. Introduction

Room temperature Ionic Liquids (ILs) are a very broad class of chemical compounds, most commonly composed of organic cations and organic or inorganic anions, whose first ever mention dates back to the early 1900s [1]. These systems usually present high thermal and chemical stability, low vapor pressure, high thermal and electrical conductivity and retain their liquid state for a wide range of temperatures [2–5].

* Corresponding author at: HyLab - Green Hydrogen Collaborative Laboratory, Edifício da Quinta da Lameira, Sines Tecnopolo, ZIL II, Lote 122A, 7520-309 Sines, Portugal.
E-mail address: maria.beira@tecnico.ulisboa.pt (M.J. Beira).

https://doi.org/10.1016/j.molliq.2025.127892
Received 4 February 2025; Received in revised form 27 May 2025; Accepted 31 May 2025
Available online 11 June 2025

Moreover, given the numerous possible cation-anion combinations, ILs can be engineered so that they display a set of optimized properties for different applications, namely electrochemistry, gas storage, catalysis and separation processes [6–16].

The field of ionic liquids has expanded to overlap the field of other types of chemical compounds like polymers, liquid crystals and magnetic liquids, just to name a few [17–19]. As a consequence, the properties of ILs can be further extended to include the high molecular organization of liquid crystals (ionic liquid crystals) or the magnetic field responsiveness of magnetic materials, such as Magnetic Ionic Liquids (MILs).

Experimental techniques based on Nuclear Magnetic Resonance (NMR) take advantage of atomic nuclei characterized by a non-zero spin and, consequently, by a magnetic moment. Placing a sample containing NMR-active nuclei in a magnetic field gives rise to a net nuclear magnetization arinsing from nuclear moments that precess about the external magnetic field vector with a characteristic Larmor frequency that depends both on the external magnetic field and on the target nucleus (^{1}H in the case of the present study) [20]. NMR-based techniques always rely on the application of radio frequency pulses in resonance with the Larmor frequency of the target nucleus so as to perturb the magnetization and enable relaxometry and spectroscopy studies of materials, be they fluids, solids or mixtures thereof. For Magnetic Resonance Imaging (MRI) and NMR diffusometry it is further necessary to include magnetic field gradient pulse sequences to enable spacial encoding of the target nuclear spins [21].

NMR relaxometry has been widely used to study the molecular dynamics in a large variety of systems, including magnetic and non-magnetic ionic liquids, contrast agents, polymers, liquid crystals, confined systems, among others [22–28]. This technique consists in the measurement of the magnetization vector characteristic relaxation times across a broad Larmor frequency range, which leads to an NMR dispersion (NMRD) profile that encodes information on a multitude of relaxation mechanisms occurring at different spacio-temporal scales. For example, ^{1}H-NMR relaxometry is sensitive to slower dynamical processes, such as collective motions and translational self-diffusion, and also to very fast molecular rotations.

NMR relaxometry is especially sensitive to the presence of a paramagnetic species and to dynamic interactions between its unpaired electrons and the target nuclei, which explains the use of gadolinium-based systems as contrast agents for MRI. Paramagnetic relaxation may be induced when the target nucleus temporarily binds to the paramagnetic center (inner-sphere interaction) or simply diffuses in its vicinity (outer-sphere interaction) [29]. Most commonly there is a coexistence of both these processes and their deconvolution is non-trivial, often requiring the use of complementary experimental techniques, the acquisition of NMRD profiles at different temperatures and/or different metal/co-solvent concentrations [30,31,22].

A study by Gradišek et al. has proven that local orientational order might induce nuclear magnetic relaxation in simpler small-molecule-isotropic liquids, and in the isotropic phase of the 5CB liquid crystal [32]. According to this work, a system composed of amphiphilic units will always present some degree of segregation between polar and non-polar domains. Inevitably, this segregation translates into some degree of local order, which might be visible and quantifiable using NMR and X-ray techniques. Recently, local order fluctuations have also been considered in the analysis of the NMRD curves of more complex amphiphilic ionic liquids based on polycatenated cations [22,33]. Silva et al. have even been able to reach a consistent analysis of the NMRD curves obtained for phosphonium-based ionic liquids using the characteristic lengths and aggregate sizes extracted from the respective X-ray profiles [33].

In the present work, we aim to analyze a set of magnetic and non-magnetic ionic liquids based on trihexyl(tetradecyl)phosphonium chloride - $[P_{6,6,6,14}][Cl]$- and trihexyl(tetradecyl)phosphonium hexachlorogadolinium - $[P_{6,6,6,14}]_3[GdCl_6]$- using ^{1}H NMR relaxometry, particularly involving the measurement of the spin-lattice (longitudinal) relaxation rate, R_1, and diffusometry techniques, along with wide angle X-Ray diffraction, Molecular Dynamics (MD) simulations and Electrochemical Impedance Spectroscopy (EIS). The combined use of these experimental and theoretical techniques enables the study of structural and dynamical properties of the phosphonium-based ionic liquid systems, as well as of the effect of different gadolinium concentrations and different temperatures both on the size of the locally ordered aggregates and on the induced paramagnetic relaxation enhancement.

2. Experimental

2.1. Materials

The synthesis of the $[P_{6,6,6,14}]_3[GdCl_6]$ magnetic ionic liquid was made at the Research Institute for Medicines (iMed.ULisboa), according to the procedures described in the literature [34,35]. Since the presence of gadolinium has a very significant shortening effect on the longitudinal and transverse relaxation times, the magnetic ionic liquid was diluted in the non-magnetic reference $[P_{6,6,6,14}][Cl]$, based on the same cation. In Fig. 1 are presented the structure of the $[P_{6,6,6,14}]^+$ cation, obtained using the software *Avogadro* [36], and the schematic representation of the analyzed magnetic and non-magnetic ionic liquids.

For each of the three studied IL/MIL mixtures, the average molar mass, density, ^{1}H density, molar concentration of gadolinium and water content are presented in Table S1 of the supplementary materials.

2.2. Methods

X-Ray Diffractometry: X-Ray profiles were obtained using the powder method with 1.5 mm rotating capillaries. The measurements were performed using a computer controlled data acquisition system paired with an INEL CPS 590 gas curved counter and a variable-geometry setup equipped with a Max-Flux Optic graded multi-layer monochromator (CuKα radiation with $\lambda = 1.54056$Å). The background noise was estimated by making a measurement on an empty 1.5 mm capillary tube and subsequently removed from the X-Ray profiles before the model fitting analysis and calculations to determine the characteristic distances, d, and aggregate sizes, ξ, of the studied systems (details in the supplementary materials). The measurements were performed at several temperatures from 25 to 100 °C. It was not possible to acquire the X-ray profiles at 5 °C due to experimental setup limitations which did not allow to cool the studied systems to this temperature.

NMR Diffusometry: The Pulsed Gradient Stimulated Echo (PGSTE) sequence was applied to determine the self-diffusion coefficient, D. The measurements were performed using a Bruker Diff 30 probe, capable of producing a maximum 1710 G cm^{-1} magnetic field gradient strength, paired with a Bruker 7T superconducting magnet connected to a Bruker Avance III NMR console. The temperature was controlled with a precision of ±0.2 °C using the spectrometer thermocouple system. Given the biexponential behavior observed for the systems studied in this work, the attenuation of the free induction decay (FID) signal was fitted by equation (1),

$$I = I_0\, c\, exp\left\{-\gamma_{^1\mathrm{H}}^2 g^2 D_{fast}\delta^3\left(\frac{\Delta}{\delta}-\frac{1}{3}\right)\right\} + I_0\,(1-c) \times exp\left\{-\gamma_{^1\mathrm{H}}^2 g^2 D_{slow}\delta^3\left(\frac{\Delta}{\delta}-\frac{1}{3}\right)\right\}, \quad (1)$$

where $\gamma_{^1\mathrm{H}}$ is the proton gyromagnetic ratio, g is the field gradient strength, δ is the duration of the gradient pulses, Δ is the inter gradient pulse delay and c is the relative weight of the fast component of the signal.

Additionally, ^{31}P PGSTE experiments were also conducted at 11.7T, using a Bruker superconducting magnet paired with a Bruker Diff 30 probe and a Bruker Avanace III NMR console, for comparison with the MD simulation results.

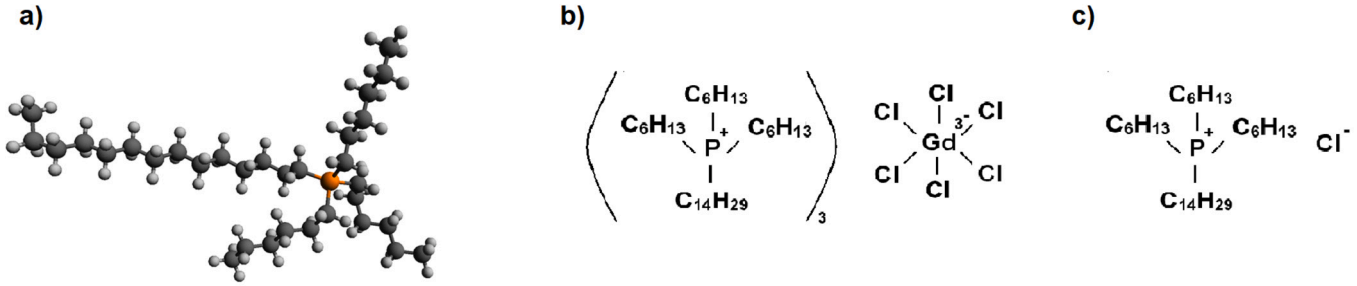

Fig. 1. a) - $[P_{6,6,6,14}]^+$ion structure obtained using *Avogadro* - b) - $[P_{6,6,6,14}]_3[GdCl_6]$ structure - c) - $[P_{6,6,6,14}][Cl]$ structure.

Molecular Dynamics (MD) Simulations: Atomistic simulations were conducted for $[P_{6,6,6,14}][Cl]$ using Gromacs 2020.6 [37] with the CL&Pol [38] force field, incorporating a drude particle scheme. Lennard-Jones parameters of the original CL&P force field [39] were adjusted using Goloviznina et al.'s approach to accommodate explicit polarization [38]. Simulations were performed in cubic boxes with 300 ion pairs, equilibrated at 100 °C for 2 ns, followed by 1 ns equilibration at each temperature (5, 25, 37, 70, and 100°C) before a 5 ns production run in the NpT ensemble. Topology files were generated using DLPGen v3.0.5 [40] and the full set of parameters can be found under the supplementary materials, along with a more comprehensive description of the simulation details. Visualization of the simulation trajectories was made with VMD 1.9.4. [41].

^{1}H NMR Relaxometry: The spin-lattice relaxation time, T_1, was measured within a ^{1}H Larmor frequency range from 10 kHz to 300 MHz, using three different NMR setups and two experimental techniques. The conventional inversion-recovery pulse sequence was applied for frequencies above 10 MHz using a Bruker Avance II console paired either with a variable field iron-core Bruker BE-30 electromagnet or a Bruker Widebore 7T (300 MHz) superconducting magnet. For frequencies below 10 MHz, T_1 was measured using the Fast Field Cycling (FFC) technique on a home-developed relaxometer having a 0.2T detection field and a switching time of $\tau_{switch} = 2.5$ ms [42]. The temperature was controlled in order to ensure that fluctuations would not exceed 0.5 °C. The magnetization curves that resulted from the relaxometry experiments were fitted to a single exponential function in order to extract the value of the spin-lattice relaxation time.

Electrochemical Impedance Spectroscopy, EIS: In order to assess the electrical properties of the $[P_{6,6,6,14}][Cl]$ ionic liquid, the compound was inserted in an ITO coated glass cell that was treated to induce planar alignment. This cell, which works as a parallel plate capacitor with a 25 mm^2 plate area and an inter plate distance of 9μm, was connected with a series resistance and kept at a fixed temperature. By controlling the voltage applied to this circuit and measuring the current, it is possible to calculate its impedance/admittance and, based on the frequency response of this parameter, reach an equivalent circuit for the compound inside the cell.

For each frequency, the applied voltage was linearly increased and then decreased in order to verify whether there was some hysteresis associated with the system. Frequencies ranging from 1 kHz to 300 kHz were tested and this experiment was performed both at 25 °C and at 70 °C.

Model Fitting:All fits were performed using the open-access online platform *fitteia*®, which applies the non-linear least squares minimization method with either an individual or global minimum target, provided by the numerical routine MINUIT from the CERN library [43–45].

Table 1
Characteristic distances and aggregate sizes extracted from the X-Ray profiles obtained at different temperatures for the samples $[P_{6,6,6,14}][Cl]$ + 0.1%(v/v) $[P_{6,6,6,14}]_3[GdCl_6]$. The presented uncertainties were estimated using the model fitting χ^2 as an estimator of the variance. Corresponding characteristic distances obtained from the molecular dynamics simulations of the neat $[P_{6,6,6,14}][Cl]$ ionic liquid.

Temperature	Large q			Small q		
	d_1 (Å)	d_1^{MD}(Å)	$\xi_\perp$ (Å)	d_2 (Å)	d_2^{MD} (Å)	$\xi_\parallel$ (Å)
5 °C	–	4.4	–	–	15	–
25 °C	4.4±0.1	4.4	9±2	18±1	16	21±5
37 °C	4.4±0.1	4.5	9±2	18±1	16	21±6
70 °C	4.5±0.1	4.5	8±2	18±1	16	19±5
100 °C	4.5±0.1	4.6	8±2	18±2	17	18±4

3. Results and discussion

3.1. X-ray diffractometry and MD simulations

The $[P_{6,6,6,14}][Cl]$ + 0.1%(v/v) $[P_{6,6,6,14}]_3[GdCl_6]$ X-Ray diffractometry results obtained at different temperatures are presented in Fig. 2. In Fig. 2a), the profiles, normalized to the number of counts and without the background contribution, were vertically shifted to enable a clearer visualization of each data set. The same was done in Fig. 2b), for the neat $[P_{6,6,6,14}][Cl]$ X-ray diffractometry profiles obtained from the MD simulations. For the results obtained at 100 °C, Figs. 2a) and b) additionally show the model fitting curve and the separate Lorentzian contributions obtained for the two existing peaks.

Following the model fitting analysis, the values obtained for the characteristic distances and aggregate sizes of the studied systems can be accessed in Table 1. A representation of the evolution of these parameters with temperature is presented in Fig. S2 in the supplementary materials file.

The results show a peak in the large q region, associated with a distance, d_1, of about 4.5Å, which is very commonly observed both in organized and non-organized liquid systems and relates to the average lateral distance between molecules. In this case, however, it is important to note that the $[P_{6,6,6,14}]^+$ ion is composed of four aliphatic chains, meaning that, as previously pointed out by Cordeiro et al. [22], this distance represents the lateral distance between aliphatic chains and not between cations.

The small q range reveals a peak that appears as a result of polar-apolar nano-segregation leading to local aggregates as the one represented in Fig. 3. Taken from *Avogadro*, the length of the longest aliphatic chain is around 16.5 Å, while the smaller aliphatic chains extend to 8Å. The characteristic distances, d_2, indicate that the 14-carbon long aliphatic chains have to penetrate adjacent layers, unlike what was observed for the $[Aliquat]^+$-based ionic liquids reported in the literature [22].

It is worth noting that, as suggested by the experimental and MD simulation results, these systems do not significantly lose their structural properties for temperatures up to 100 °C, in good agreement with what was observed for other $[P_{6,6,6,14}]^+$-based ionic liquids [46].

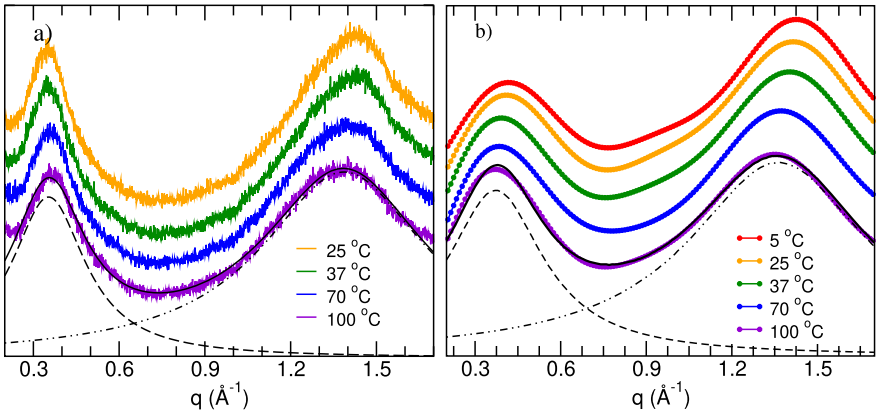

Fig. 2. Vertically shifted X-Ray diffractometry profiles obtained experimentally at different temperatures for the $[P_{6,6,6,14}][Cl] + 0.1\%(v/v)\ [P_{6,6,6,14}]_3[GdCl_6]$ system (a) and resulting from the MD simulations for $[P_{6,6,6,14}][Cl]$ (b).

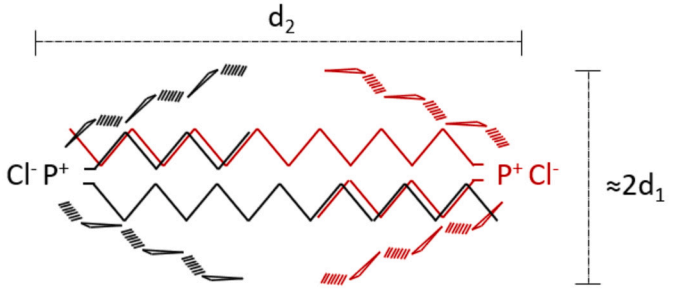

Fig. 3. Schematic representation of the aggregates formed by the $[P_{6,6,6,14}]^+$ cations. The distances d_1 and d_2 are related to the X-ray characteristic distances presented in Table 1.

As it can be observed in Fig. 2, the MD simulations reproduce well the key features of the experimentally obtained X-ray diffractograms. A polarizable model was deemed necessary to capture both the structural and dynamic properties of this ionic liquid with highly localized charges.

A snapshot corresponding to the final configuration of $[P_{6,6,6,14}][Cl]$ at 25 °C is shown in Fig. 4. There, we can see that phosphorus (orange) and chlorine (green) atoms are alternatingly interconnected throughout the simulation box in a thread-like polar network. This polar network, similar to what is observed in other families of compounds such as imidazolium-based ILs [47], is characterized by the formation of strong ion pairs [48], as demonstrated by the sharp peak in the heteroatomic P-Cl radial distribution function (Fig. S3). The large interstitial spaces are occupied by the hydrocarbon chains, represented in gray color, forming a reciprocal apolar network that also percolates the simulation box.

The MD simulations provide more insights on the structural properties of the studied systems. Additional information regarding the molecular organization in the $[P_{6,6,6,14}][Cl]$ ionic liquid, including the radial distribution functions and the intramolecular distribution of distances, is available in the supporting information.

3.2. Diffusometry - MD simulations and PGSTE NMR

Apparent diffusivities were calculated from the MD simulation trajectories, and the results are presented in Table 2. Overall, the coefficients obtained for the $[P_{6,6,6,14}][Cl]$ ionic liquid are relatively well predicted by the polarizable model. In particular, the value at 25 °C is within the range reported by Mendivelso-Pérez et al. (0.98 - 1.2 $\mu m^2/s$) [49] and it is also in close proximity to the values measured using PGSTE NMR diffusometry.

As it can be seen in Table 2, the Cl^- ion diffuses at a very similar pace to the phosphorus atom, as they are intertwined along the polar network. Interestingly, the cation as a whole presents a higher diffusion coefficient, very similar to the entire system, meaning that the hydrocarbon chains have some freedom to move despite being anchored to the slow-moving P center. The relative motion between the cations and the anions in these phosphonium salts would be very difficult to obtain experimentally using NMR due to the chlorine nuclear quadrupole spin moment.

Table 2
Apparent diffusivities obtained for the ionic liquid $[P_{6,6,6,14}][Cl]$ the cation $[P_{6,6,6,14}]^+$, the anion $[Cl]^-$ and the phosphorus atom P. The results obtained by PGSTE NMR at 25 °C are also presented.

Temperature		$D^a_{[P_{6,6,6,14}][Cl]}$	$D^a_{[P_{6,6,6,14}]^+}$	D^a_P	$D^a_{Cl^-}$
		$10^{-12} m^2/s$			
5 °C		0.5±0.4	0.5±0.4	0.2±0.2	0.2±0.2
25 °C		1.1±0.4	1.1±0.4	0.4±0.2	0.4±0.1
	NMR	–	1.5 ±0.1	0.4 ±0.1	–
37 °C		1.5±0.4	1.5±0.4	0.4±0.3	0.3±0.2
70 °C		4±1	4±1	1.2±0.2	1.2±0.1
100 °C		8±2	9±2	3.6±0.3	3.0±0.6

In Fig. S5 of the supplementary materials are presented the evolution of the mean square displacement with the simulation time obtained for the cation and the anion at different temperatures.

Given the NMR spectrum deformation observed for the paramagnetic systems (details in the supporting information), the diffusion coefficients obtained by PGSTE NMR were not considered in the model fitting analysis of the ^1H NMR relaxometry results that are presented in the following section.

3.3. ^1H NMR relaxometry

The experiments performed at different ^1H Larmor frequencies allowed for the determination of the respective spin-lattice relaxation rates, $R_1 = T_1^{-1}$, which compose the NMR dispersion (NMRD) curves. In order to fit the NMRD curves obtained for the $[P_{6,6,6,14}][Cl]$ reference sample, as well as for each paramagnetic mixture, it was considered that relaxation could happen as a result of rotations/reorientations (Rot), translational diffusion (SD), local order fluctuations (OPF), cross-relaxation with the chloride ions (CR) and, in the case of gadolinium containing samples, inner and outer sphere paramagnetic relaxation (PM) [50,51,22]. The order parameter fluctuations model, generally applied to liquid-crystalline systems, is needed to account for the presence of locally ordered domains arising both from the amphiphilic and anisometric character of the studied systems, as suggested by the X-ray diffractometry results. This model was proven to be needed for the interpretation of ^1H NMR relaxometry data of similar non-liquid-crystalline ionic liquid systems [22,33]. The considered relaxation mechanisms, detailed in the supplementary materials, were assumed to act within

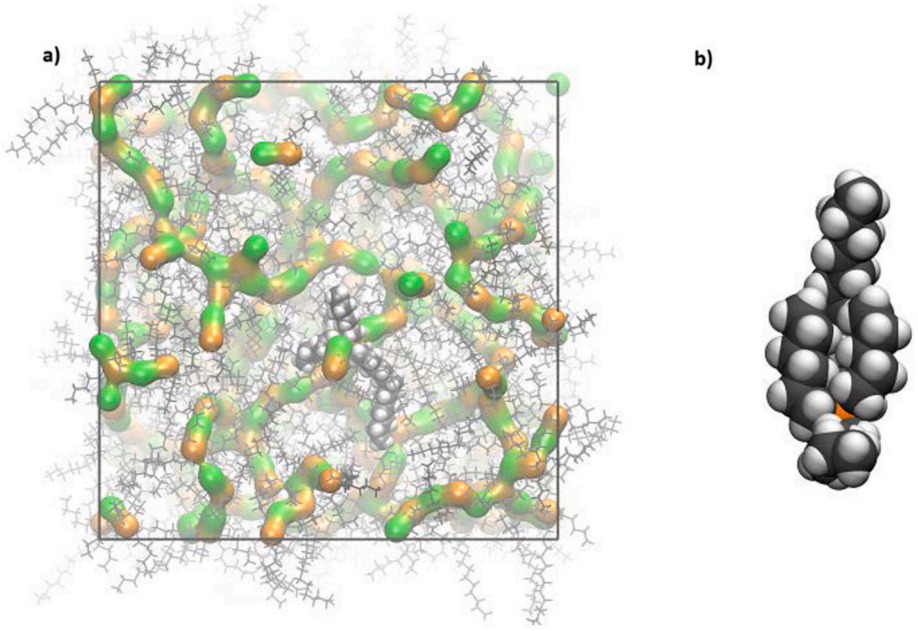

Fig. 4. a) MD simulation snapshot of the final configuration of $[P_{6,6,6,14}][Cl]$ at 25 °C, showing the polar network formed by phosphorous (orange) and chlorine (green) atoms. b) MD conformation of a $[[P_{6,6,6,14}]^+$ cation displaying strong self-interactions between the hydrocarbon chains. Carbon atoms are colored gray, hydrogens white, phosphorus orange and chlorine green.

independent timescales [52], which allows the total relaxation rate to be a sum of the aforementioned individual contributions, as described in equation (2)

$$\frac{1}{T_1} = \frac{1}{T_1^{Rot}} + \frac{1}{T_1^{SD}} + \frac{1}{T_1^{OPF}} + \frac{1}{T_1^{CR}} + \frac{1}{T_1^{PM}}. \quad (2)$$

The model fitting analysis was made simultaneously for all studied samples (magnetic and non-magnetic) and all temperatures.

In Fig. 5 are presented the NMRD and model fitting curves, as well as the independent model contributions, obtained for the reference $[P_{6,6,6,14}][Cl]$ sample at 5, 25, 37 and 70 °C. Table 3 shows the values obtained for the corresponding model fitting parameters.

The parameters' uncertainties were estimated by testing the sensitivity of the fit to each parameter individually, except for parameters τ_{Rot} and A_{OPF}, whose uncertainties were propagated given the assumed Arrhenius thermal activation characterized by $\tau_{Rot_{ref}}$ =(1.34±0.06) $\times 10^{-10}$ s and $E\tau_{Rot}$ =(30±2) kJ/mol and $A_{OPF_{ref}}$ =(1.93±0.07) $\times 10^5$ $s^{-3/2}$ and EA_{OPF} =(13±2) kJ/mol, respectively. The reference values are related with a 25 °C temperature.

As it can be observed in Fig. 5, the model fitting analysis of the reference non-magnetic sample provided very good global fits considering equation (2) and using as few parameters as possible. The SD contribution is more significant across the lower frequency range, while, for intermediate to high frequencies, the OPF relaxation mechanism becomes the most significant. Only at high frequencies is it possible to estimate the contribution describing fast rotations/reorientations.

This model fitting analysis also takes into account the experimental X-ray diffractometry and ^{1}H NMR diffusometry results. The translational diffusion contribution obtained by equalizing the lateral intercation distance, d, and the mean square jump distance, r, for all temperatures, in accordance with the negligible temperature dependence of the X-ray profiles, resulted in translational diffusion coefficients consistent with those measured by ^{1}H PGSTE NMR. Additionally, using the X-ray characteristic distances and aggregate sizes related to the peak in the small q region of the diffractograms (see Table 1), it was possible to fix the relation between the minimum and maximum cutoff frequencies related to the OPF model contribution to those presented in Table 3. This method had previously been applied by Silva et al. [33] and was successfully extended to the present multi-temperature study. More details on the model parameters' analysis can be accessed in the supplementary information.

Table 3
Parameters obtained from the NMRD fitting of the non-paramagnetic sample at different temperatures. Uncertainties were estimated by probing the sensitivity of the fit to each individual parameter, except for the rotational correlation time, τ_{Rot}, and the order fluctuations prefactor, A_{OPF}, whose uncertainties were propagated from the assumed Arrhenius thermal activation, respectively characterized by parameters $\tau_{Rot_{ref}}$ =(1.34±0.06) $\times 10^{-10}$ s and $E\tau_{Rot}$ =(30±2) kJ/mol and by $A_{OPF_{ref}}$ =(1.93±0.07) $\times 10^5$ $s^{-3/2}$ and EA_{OPF} =(13±2) kJ/mol. The ^{1}H spin density, n, needed for the Torrey model, was fixed to the value presented in Table S1, A_{Rot} was determined using *Avogadro* and computing the resulting inter-hydrogen distances and the ratio between the maximum and minimum cutoff frequencies were calculated using the characteristic distances and aggregate sizes obtained via X-Ray diffractometry, as explained in the text, with the exception of the 5 °C - related NMRD.

	Parameters	$[P_{6,6,6,14}][Cl]$			
		5 °C	25 °C	37 °C	70 °C
Rot	$A_{Rot}(10^9\ s^{-2})$	5.2			
	$\tau_{Rot}(10^{-10} s)$	3.2±0.4	1.34±0.06	0.84±0.07	0.27±0.05
SD	$D(10^{-12} m^2/s)$	≈0.7	1.60±0.03	3.3±0.5	21±8
	r(Å)	≈ 6			
	d(Å)	7.4±0.4			
OPF	$A_{OPF}(10^5\ s^{-3/2})$	2.8±0.3	1.93±0.07	1.6±0.1	1.0±0.2
	$f_{min}(10^6\ s^{-1})$	2.7±0.3	9.7±0.9	12±2	64±10
	f_{min}/f_{max}	0.17±0.02	0.18	0.19	0.22
CR	$A_{CR}(10^8\ s^{-2})$	2.2±0.4			
	$f_{CR}(10^7\ s^{-1})$	1.0±0.2			
	$\tau_{CR}(10^{-8} s)$	1.6±0.7			

When the reference $[P_{6,6,6,14}][Cl]$ sample is mixed with $[P_{6,6,6,14}]_3[GdCl_6]$, even in very small amounts, a broad peak in the high frequency range is observed. The raw relaxometry data obtained for the three studied $[P_{6,6,6,14}]_3[GdCl_6]$ concentrations can be observed in Fig. 6. The model fitting curve obtained at 70 °C was also added along with the

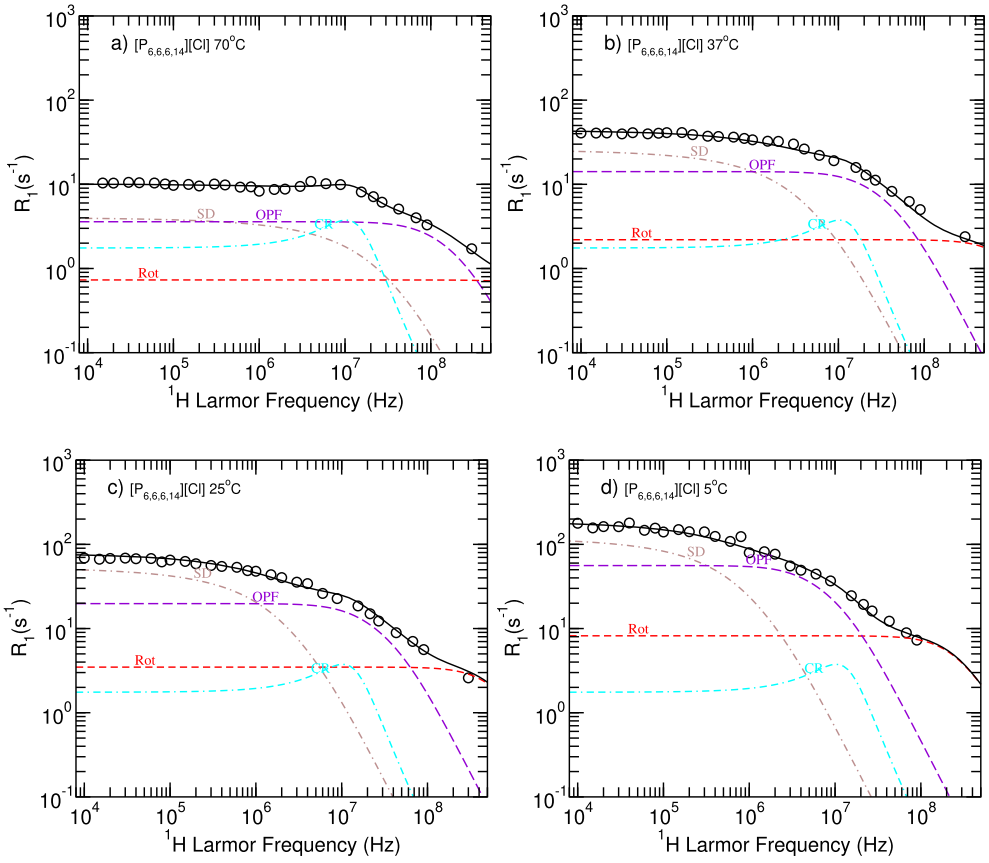

Fig. 5. NMRD, model fitting curves and separate model contributions obtained for the reference sample, $[P_{6,6,6,14}][Cl]$, at 70 °C (a), 37 °C (b), 25 °C (c) and 5 °C (d).

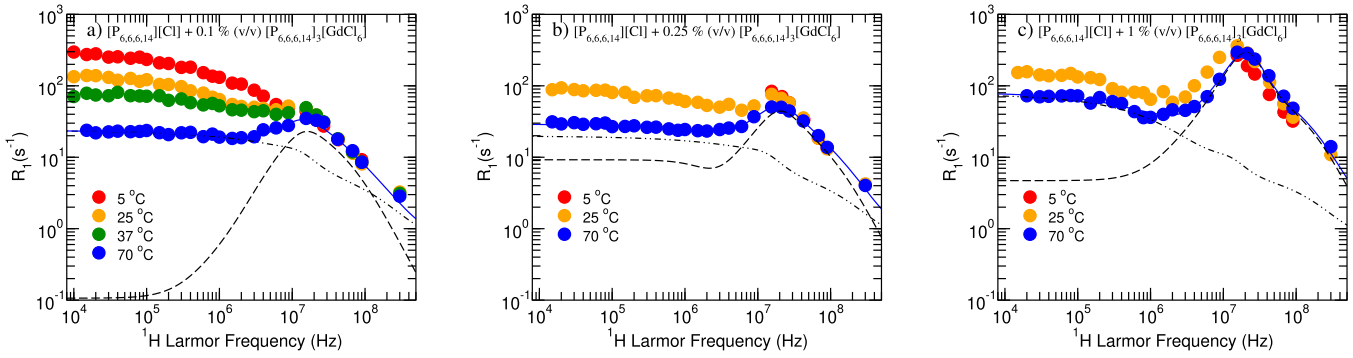

Fig. 6. NMR dispersion curves obtained for the gadolinium containing mixtures, at different temperatures. Model fitting curves obtained following the analysis of the NMRD profiles acquired at 70 °C. The dashed line relates to the PM relaxation contributions, while the dot-dot-dashed line relates to the sum of SD, OPF, CR and Rot contributions.

paramagnetic (dashed line) and non-paramagnetic (dot-dot-dashed line) relaxation contributions.

By looking at Fig. 6, it is possible to see that, as the gadolinium concentration increases, the peak in the high frequency range becomes more evident. Moreover, the results presented in Fig. 6c) show a paramagnetic relaxation enhancement comparable to the one observed by Cordeiro et al. [22] for the $[Aliquat]^+$-based systems, but achieved with 12 times lower metal concentrations, which is a promising result. The fact that gadolinium has a higher electronic spin when compared to iron and that the anionic complex where it is included binds more cations makes it better for this type of paramagnetic contrast. It is, however, important to note that the enhancement peak covers a narrower range of ^{1}H Larmor frequencies than the one observed for the $[Aliquat]^+$-based systems.

In the case of the samples containing less gadolinium in their composition (Fig. 6a) and b)), the relaxation rate for ^{1}H Larmor frequencies above 10 MHz seems to be almost independent of temperature. However, as it can be seen in the high frequency range of Fig. 6c), the sample having 1%(v/v) $[P_{6,6,6,14}]_3[GdCl_6]$ presents a significant temperature dependence, which allows to tune the frequency where the maximum relaxation rate, and, therefore, the largest contrast, occurs.

The NMRD curves obtained for the paramagnetic mixtures were fitted to the model described by equation (2). Aside from the contributions fitted to the reference $[P_{6,6,6,14}][Cl]$ sample, the model additionally considers inner-sphere, **IS**, and outer-sphere, **OS**, contributions to paramagnetic relaxation (see the theoretical model section on the supplementary materials for more information on these contributions).

In Fig. 7 are presented the model fitting curves and separate contributions obtained for the NMRD data acquired at 25 °C for all the studied gadolinium-based paramagnetic systems. Table 4 shows the model fit-

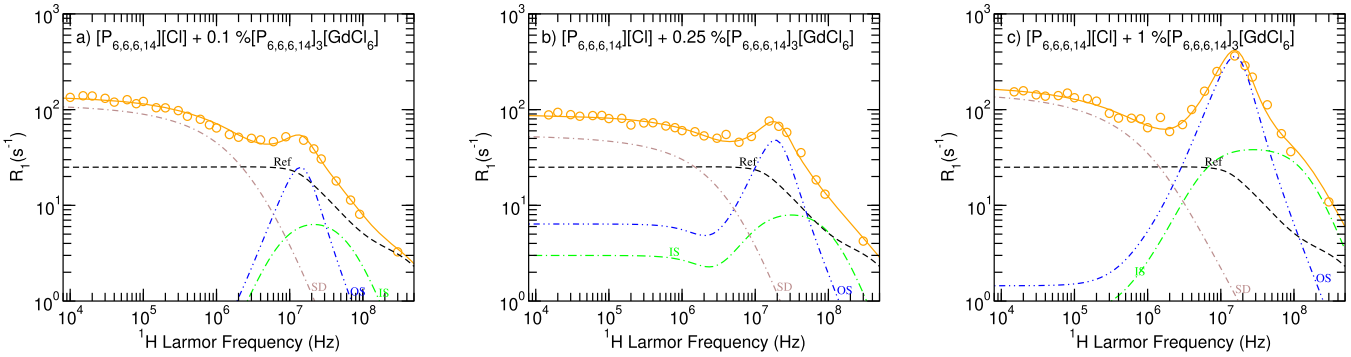

Fig. 7. NMR dispersion curves obtained for the three studied paramagnetic mixtures at 25 °C and corresponding model fitting curves. The contributions fixed from the analysis of the reference $[P_{6,6,6,14}][Cl]$ sample, namely OPF, CR and Rot, are represented by the dashed black curve. The dot-dashed brown line relates to the fitted SD contribution. The paramagnetic contributions are given by the green dot-long-dashed and by the blue dot-dot-dashed lines, representing inner- and outer sphere relaxation mechanisms, respectively.

Table 4
Parameters obtained from the NMRD fitting of the $[P_{6,6,6,14}][Cl]$ + 0.1% (v/v) $[P_{6,6,6,14}]_3[GdCl_6]$ sample at 5, 25, 37 and 70 °C and of the $[P_{6,6,6,14}][Cl]$ + 0.25% (v/v) $[P_{6,6,6,14}]_3[GdCl_6]$ and $[P_{6,6,6,14}][Cl]$ + 1% (v/v) $[P_{6,6,6,14}]_3[GdCl_6]$ samples at 25 and 70 °C. Uncertainties were estimated by probing the sensitivity of the fit to each individual parameter. The contributions from rotations, cross-relaxation and local order fluctuations were fixed to the ones obtained for the reference sample and presented in Table 3, the ^1H spin density, n, needed for the Torrey model contribution, as well as the gadolinium concentration, were fixed to the values presented in Table S1 and the electronic spin S was fixed to 7/2.

	Parameters	$[P_{6,6,6,14}][Cl]$/ 0.1% $[P_{6,6,6,14}]_3[GdCl_6]$				$[P_{6,6,6,14}][Cl]$/ 0.25% $[P_{6,6,6,14}]_3[GdCl_6]$		$[P_{6,6,6,14}][Cl]$/ 1% $[P_{6,6,6,14}]_3[GdCl_6]$	
		5 °C	25 °C	37 °C	70 °C	25 °C	70 °C	25 °C	70 °C
SD	D ($10^{-12}m^2/s$)	0.44±0.04	0.94±0.08	1.7±0.2	6.1±0.4	2.1±0.4	8±2	0.57±0.08	1.2±0.2
	r(Å)	3±1				5±3		≈ 3	
	d(Å)	5.5±0.2				5.9±0.6		6.0±0.9	
OS	d^{OS} (Å)	4.3±0.3				5.1±0.2		3.81±0.07	
	D ($10^{-12}m^2/s$)	0.44±0.04	0.94±0.08	1.7±0.2	6.1±0.4	2.1±0.4	8±2	0.57±0.08	1.2±0.2
	τ_v ($10^{-10}s$)	5±2				0.55±0.05		3.7±0.4	1.7±0.2
	Δ^2 (10^{19} s^{-2})	4±2				1.0±0.1		4.0±0.5	
IS	d^{IS} (Å)	5.3±0.2				12±2		≈ 6	
	τ_m ($10^{-9}s$)	2.4±0.8				1.4±0.5		1.1±0.2	
	τ_v ($10^{-10}s$)	5±2				0.55±0.05		3.7±0.4	1.7±0.2
	Δ^2 (10^{19} s^{-2})	4±2				1.0±0.1		4.0±0.5	

ting parameters obtained from the global multi-temperature and multi $[P_{6,6,6,14}]_3[GdCl_6]$ concentration model fitting analysis.

Both the cross-relaxation, the rotations/reorientations and the local order fluctuations contributions were fixed to those obtained for the $[P_{6,6,6,14}][Cl]$ reference sample, since they are completely masked by the remaining relaxation mechanisms, namely those related to paramagnetic relaxation. The sum of these three fixed contributions is represented by the black dashed line in Figs. 7.

Spectral deformation observed after performing PGSTE NMR on the paramagnetic samples (see supplementary materials) did not allow for a good estimation of the diffusion coefficients in these systems. However, as neither inner- nor outer-sphere relaxation are dominant mechanisms across the lower frequency range, translational self-diffusion could be estimated independently from the NMRD profiles of the paramagnetic mixtures. The analysis was made setting self-diffusion as a free parameter, but, in order to restrict the possible values, the mean square jump distance, r, and average intermolecular interspin distance, d, were considered to be temperature independent, as was previously done for the non-magnetic system.

Regarding paramagnetic relaxation, the relative diffusion coefficient in the outer-sphere contribution was assumed to be that of the cation in the fitting process. The reason for this relates with the fact that the diffusion of the paramagnetic anion is orders of magnitude smaller than that of the cation's, since it is strongly coordinated with three $[P_{6,6,6,14}]^+$ ions. This is also in line with the molecular dynamics simulations results that suggest a less mobile polar area, as opposed to the terminal aliphatic chain groups.

The parameters Δ and τ_v, common to both inner- and outer-sphere contributions, describe electron spin relaxation processes that contribute to the paramagnetic relaxation enhancement (PRE). This enhancement manifests as a high-frequency bump in the relaxometry profiles of paramagnetic mixtures. It originates from fluctuations in the zero-field splitting (ZFS) interaction caused by molecular motions. Here Δ characterizes the magnitude of these fluctuations, while τ_v represents their correlation time. [53,54,29]

In the case of these mixtures, the characteristic inner-sphere distance of closest approach is slightly smaller than the one obtained for the outer-sphere contribution. This fact may be related with the interdigitation of the 14-carbon long aliphatic chain, allowing the proximity of unbound ^1H nuclei to the paramagnetic anion to be smaller than that of directly bound ^1H nuclei, as suggested by the structure scheme presented in Fig. 3. The outer-sphere mechanism seems to be the most relevant for these systems, not only due to the very restricted translational diffusion, but also as a result of the interdigitated cation long chains. Parameters τ_v and Δ were estimated from the model fitting analysis taking into account that they should be the same for the inner and outer-sphere contributions, as reflected in Table 4. τ_v presents different results at different temperatures only for the sample having the largest amount of gadolinium, in order to explain the temperature dependence observed at the highest frequency. As Δ presents an indirect measure of the chemical environment surrounding the paramagnetic center it was allowed a

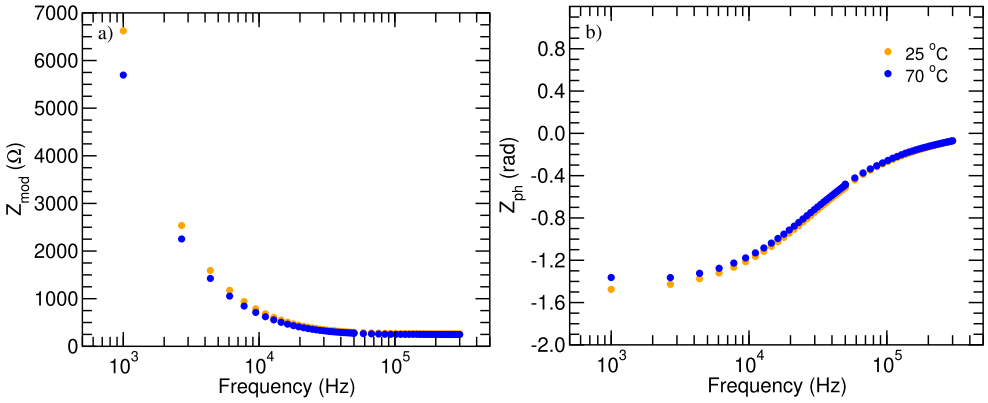

Fig. 8. Bode representation of the impedance results obtained for the studied system at 25 and 70 °C.

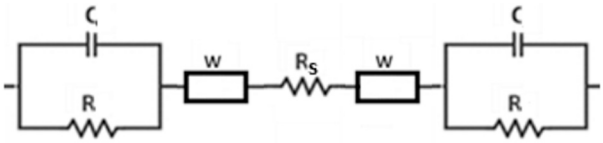

Fig. 9. Schematic representation of the $[P_{6,6,6,14}][Cl]$ and ITO-coated glass cell equivalent circuit.

different value for the $[P_{6,6,6,14}][Cl]$ + 0.25% (v/v) $[P_{6,6,6,14}]_3[GdCl_6]$ which is known to present an increased amount of water, as it can be observed in Table S1. The exchange time, τ_m, was allowed to vary for the different mixtures, but its values were kept for all temperatures.

The complete set NMRD profiles and the corresponding model fitting curves are available in the supplementary information.

3.4. Electrochemical impedance spectroscopy

Phosphonium-based salts are of interest for electrochemical applications. They might be used to integrate supercapacitor systems [55,56] and have shown promising results, for example, as an electrolyte to promote electro-synthesis of ammonia at ambient temperature and pressure [8]. It is, therefore, of interest to associate the electrochemical properties of such systems with their structural properties and their molecular dynamics.

Fig. 8 shows the impedance profiles of the analyzed $[P_{6,6,6,14}][Cl]$ ionic liquid in the ITO-coated glass cell. The profiles were acquired at two different controlled temperatures.

The analogous equivalent circuit applied to the studied ionic liquid system is presented in Fig. 9 and the respective model expression is given by equation (3), where j is the imaginary unit.

$$Z = 2\left(\frac{1}{j\omega C + \frac{1}{R}} + \frac{W}{\sqrt{j\omega}}\tanh\left(B\sqrt{j\omega}\right)\right) + R_s \quad (3)$$

The two equivalent parallel RC circuits account for charge transfer and accumulation in the electrode-electrolyte interface and were allowed to vary freely for the two studied temperatures (25 and 70 °C). The Warburg elements, also referred to as a diffusion capacitance, account for mass-transfer limitations [57,58]. Both parameters B and W are inversely proportional to the square root of the diffusion coefficient, therefore, they were forced to vary equivalently with temperature. More precisely, the parameters B and W for the data obtained at 70 °C are those obtained for 25 °C multiplied by a common factor. Parameter B becomes important for restricted diffusion, which was observed to be the case for the $[P_{6,6,6,14}][Cl]$ ionic liquid across the studied temperature and frequency range. The fact that the Warburg impedance appears in the circuit as an independent element, for instance not in parallel to any resistor, might be a consequence the fact that charge migration due to the electric field is less significant when compared with charge self-diffusion, which makes sense in view of the fact that the charges are localized on one end of the more mobile and non-polar aliphatic chains. Other works have also used this element independently [59,60]. Last, the element R_s represents the bulk solution resistance.

As the equivalent impedance of a series of circuit blocks is the sum of the impedance of each block, it is advantageous to represent the real and imaginary parts of the impedance as a function of frequency, as this allows the individual contributions to be visualized. In Fig. 10 are presented the results of the global fit of the profile pairs obtained at 25 and 70 °C.

As it can be observed, the profiles are mostly explained by the RC circuit blocks and the R_s resistance. At 70 °C, R becomes smaller while C becomes larger. This is consistent with a reduction of the electrochemical double layer thickness for increasing temperatures. The bulk resistance, R_s, was a common parameter for both temperatures, which might indicate that it associates more with the local aggregate structure. As shown in the X-Ray diffractometry study, this local order is almost unaffected by temperature within the temperature range where impedance was evaluated.

Regarding the Warburg element, it was possible to fit the data assuming that W and B vary with temperature solely as a result of the different diffusion coefficients. The factor obtained appears to indicate that diffusion varies less than what was suggested by the NMR results or calculated through MD simulations. This could be explained, not only by the fact that surface interactions become important in such a narrow glass cell and these would not be captured by NMR or MD simulations, but also because the NMR measured self-diffusion coefficients are prone to overestimation due to the relative motion of the mobile end groups of the aliphatic chains. It could be argued that the fit would be possible without considering this element, in view of its relatively small importance when compared with the remaining circuit blocks, however, as it can be observed in Fig. S9 of the supplementary materials, this contribution is relevant to explain the data points in the kHz frequency range.

4. Conclusions

In this comprehensive research work, we investigated the molecular dynamics of magnetic and non-magnetic ionic liquids based on the $[P_{6,6,6,14}]^+$ ion. Specifically we studied a non-magnetic reference, $[P_{6,6,6,14}][Cl]$, and three mixtures of the reference compound with 0.1, 0.25 and 1% (v/v) of $[P_{6,6,6,14}]_3[GdCl_6]$. It was absolutely necessary to use very diluted amounts of MIL in order to enable this study, since the presence of the paramagnetic species very significantly reduces the relaxation times.

The obtained results show that it is necessary to consider local order fluctuations as a relaxation mechanism in order to obtain quantitatively consistent results relating the temperature dependent relaxometry data with the corresponding structure information obtained from X-ray

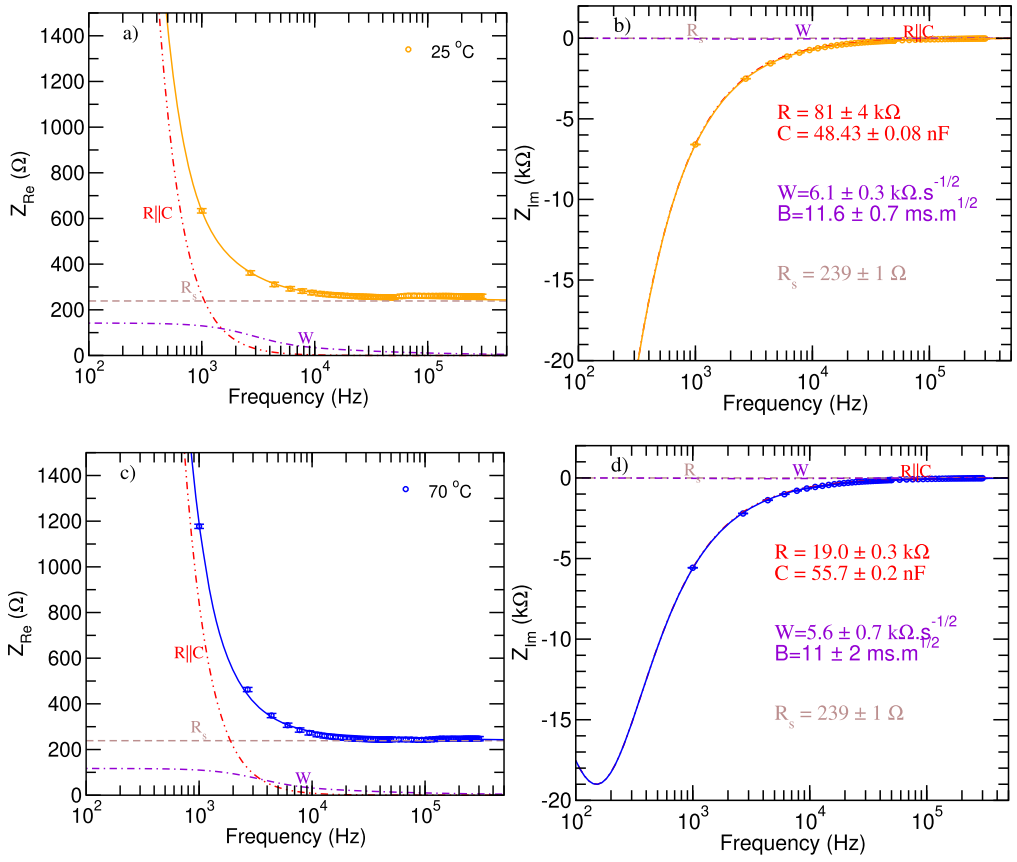

Fig. 10. Impedance real - a), c) - and imaginary -b),d) - parts in function of frequency, along with the model fitting analysis curves and parameters. The dot-dot-dashed red line represents the RC parallel circuit block, the brown dashed line relates to R_s and dot-dashed violet curve relates to the diffusion capacitance elements. The uncertainties were estimated after normalizing the χ^2 to the number of degrees of freedom.

diffractometry and MD simulations. In particular, the existence of local aggregates enables the estimation of the ratio between the minimum and maximum cutoff frequencies of the order parameter fluctuation relaxation model, thus decreasing the number of free model fitting parameters.

The diffusion coefficient calculations using MD simulation results, corroborated by experimental PGSTE ^{1}H and ^{31}P NMR diffusometry, indicate that the $[P_{6,6,6,14}]^+$ cation presents an apparent diffusion coefficient that is larger for the ^{1}H nuclei, due to the more mobile aliphatic chains' terminal groups, than for the phosphorus charge center. Additionally, MD simulations were particularly useful to access the relative anion-cation dynamics, which would be very difficult to obtain experimentally.

The paramagnetic relaxation enhancement produced by the presence of $[P_{6,6,6,14}]_3[GdCl_6]$ presented some interesting features, namely the fact that the inner-sphere distance of closest approach is larger than the characteristic distance obtained for the outer-sphere mechanism. This result can be explained by the interdigitation of the longest aliphatic chain, whose hydrogen nuclei can move closer to the paramagnetic center than those coordinated with it (i.e. those belonging to the bound cations). The relaxation enhancement obtained is very significant, taking into consideration the very small concentrations of Gadolinium used in the mixtures (maximum 1mM), which may be explained both by this lanthanide's high electronic spin and by the fact that the metallic anionic complex bounds three highly protonated cations. Moreover, the magnetic field corresponding to the maximum relaxation enhancement can be tuned by changing the temperature.

The impedance profiles of the $[P_{6,6,6,14}][Cl]$ ionic liquid were additionally evaluated. The contribution of the different circuit elements could be deconvoluted using the representation of the real and imaginary parts of the impedance in function of frequency. The obtained results allowed for a consistent global analysis considering both the locally ordered aggregates characterized by X-ray diffractometry and MD simulations, and the diffusometry results.

Conjointly, the results obtained in the present work enabled a fundamental analysis that allowed for understanding the structural, dynamical, electrical and paramagnetic properties of $[P_{6,6,6,14}]^+$based magnetic and/or non-magnetic ionic liquid systems. We expect these results to contribute for the design of systems with optimized properties for different applications.

CRediT authorship contribution statement

Maria J. Beira: Writing – review & editing, Writing – original draft, Investigation, Formal analysis, Conceptualization. **Gonçalo M.C. Silva:** Writing – review & editing, Investigation, Conceptualization. **Tiago M. Eusébio:** Writing – review & editing, Investigation, Conceptualization. **João L. Figueirinhas:** Writing – review & editing, Supervision, Resources, Investigation, Conceptualization. **Rui Cordeiro:** Writing – review & editing, Investigation, Conceptualization. **Carlos Cruz:** Writing – review & editing, Supervision, Investigation, Conceptualization. **Marta C. Corvo:** Writing – review & editing, Resources, Investigation, Conceptualization. **Pedro L. Almeida:** Writing – review & editing, Resources, Investigation, Conceptualization. **Andreia A. Rosatella:** Writing – review & editing, Resources, Conceptualization. **Carlos A.M. Afonso:** Writing – review & editing, Resources, Conceptualization. **Eduardo J.M. Filipe:** Writing – review & editing, Supervision, Conceptualization. **Teodor Parella:** Writing – review & editing, Supervision, Conceptualization. **Eurico J. Cabrita:** Writing – review & editing, Supervision, Conceptualization. **Pedro J. Sebastião:** Writing – review & editing, Supervision, Software, Formal analysis, Conceptualization.

Declaration of competing interest

The authors declare that they have no known competing financial interests or personal relationships that could have appeared to influence the work reported in this paper.

Acknowledgements

The authors would like to thank European COST Action EURELAX CA15029 (2016-2020) and Carla I. Daniel for the initial contributions, namely providing the paramagnetic mixtures and measuring water content, and for allowing use of the setups to measure the systems density and viscosity. For enabling the diffusometry studies at 11.7T, the authors also acknowledge Maria João Ferreira and José Acenso for access to the CQE NMR laboratory at Instituto Superior Técnico, Lisbon. M.C.C. gratefully acknowledges PTNMR for the researcher contract. This work was supported by Fundação para a Ciência e Tecnologia through projects: UID/CTM/04540/2019, UID/CTM/50025/2019, UID/DTP/04138/2020, UID/QUI/50006/2019, UIDB/50025/2020-2023 and PTNMR (2017-2020); and European Commission project M-ERA-NET2/0006/2019 (2017-2020) CELLCOLOR. Author M.J.B also received Ph.D. scholarship PD/BD/142858/2018 and scholarship extention COVID/BD/152743/2022. The NMR spectrometers at IST and FCT NOVA are part of the National NMR network (PTNMR). They are partially supported by Infrastructure Project no. 022161 (co-financed by FEDER through COMPETE 2020, POCI and PORL and FCT through PIDDAC) and additionally by FCT (ROTEIRO/0031/2013-PINFRA/22161/2016). CBIOS, Universidade Lusófona acknowledges FCT for funding projects DOI reference 10.54499/UIDB/04567/2020 and 10.54499/UIDP/04567/2020, and 10.54499/EXPL/OCE-ETA/1109/2021. Projects LA/P/0037/2020, UIDP/50025/2020 and UIDB/50025/2020 of the Associate Laboratory Institute of Nanostructures, Nanomodelling and Nanofabrication-i3N are also acknowledged.

Appendix A. Supplementary material

Supplementary material related to this article can be found online at https://doi.org/10.1016/j.molliq.2025.127892.

Data availability

Data will be made available on request.

References

[1] P. Walden, Molecular weights and electrical conductivity of several fused salts, Bull. Acad. Imp. Sci. St.-Pétersbg. (1914).
[2] E. Santos, J. Albo, A. Irabien, Magnetic ionic liquids: synthesis, properties and applications, RSC Adv. 4 (2014) 40008–40018, https://doi.org/10.1039/C4RA05156D.
[3] M. Earle, J. Esperanca, M. Gilea, J. Lopes, K. Seddon, J. Magee, J. Widegren, The distillation and volatility of ionic liquids, Nature 439 (2006) 831–834, https://tsapps.nist.gov/publication/get_pdf.cfm?pub_id=50194.
[4] A. Abo-Hamad, M.A. AlSaadi, M. Hayyan, I. Juneidi, M.A. Hashim, Ionic liquid-carbon nanomaterial hybrids for electrochemical sensor applications: a review, Electrochim. Acta 193 (2016) 321–343, https://doi.org/10.1016/j.electacta.2016.02.044, https://www.sciencedirect.com/science/article/pii/S0013468616303097.
[5] A.R. Hajipour, F. Rafiee, Basic ionic liquids. A short review, J. Iran. Chem. Soc. 6 (2009) 647–678.
[6] M. Ishikawa, T. Sugimoto, M. Kikuta, E. Ishiko, M. Kono, Pure ionic liquid electrolytes compatible with a graphitized carbon negative electrode in rechargeable lithium-ion batteries, J. Power Sources 162 (1) (2006) 658–662.
[7] G.M.A. Girard, M. Hilder, H. Zhu, D. Nucciarone, K. Whitbread, S. Zavorine, M. Moser, M. Forsyth, D.R. MacFarlane, P.C. Howlett, Electrochemical and physicochemical properties of small phosphonium cation ionic liquid electrolytes with high lithium salt content, Phys. Chem. Chem. Phys. 17 (2015) 8706–8713, https://doi.org/10.1039/C5CP00205B.
[8] F. Zhou, L.M. Azofra, M. Ali, M. Kar, A.N. Simonov, C. McDonnell-Worth, C. Sun, X. Zhang, D.R. MacFarlane, Electro-synthesis of ammonia from nitrogen at ambient temperature and pressure in ionic liquids, Energy Environ. Sci. 10 (2017) 2516–2520, https://doi.org/10.1039/C7EE02716H.
[9] D. Tempel, P. Henderson, J. Brzozowski, R. Pearlstein, H. Cheng, High gas storage capacities for ionic liquids through chemical complexation, J. Am. Chem. Soc. 130 (2) (2008) 400–401.
[10] E. Santos, J. Albo, A. Rosatella, C.A. Afonso, A. Irabien, Synthesis and characterization of magnetic ionic liquids (mils) for co2 separation, J. Chem. Technol. Biotechnol. 89 (6) (2014) 866–871, https://doi.org/10.1002/jctb.4323, https://onlinelibrary.wiley.com/doi/abs/10.1002/jctb.4323.
[11] L.M. dos Santos, F.L. Bernard, B.B. Polesso, I.S. Pinto, C.C. Frankenberg, M.C. Corvo, P.L. Almeida, E. Cabrita, S. Einloft, Designing silica xerogels containing rtil for co2 capture and co2/ch4 separation: influence of ils anion, cation and cation side alkyl chain length and ramification, J. Environ. Manag. 268 (2020) 110340, https://doi.org/10.1016/j.jenvman.2020.110340, https://www.sciencedirect.com/science/article/pii/S0301479720302759.
[12] M. Ramdin, T.W. de Loos, T.J. Vlugt, State-of-the-art of co2 capture with ionic liquids, Ind. Eng. Chem. Res. 51 (24) (2012) 8149–8177, https://doi.org/10.1021/ie3003705.
[13] J. Sun, W. Cheng, W. Fan, Y. Wang, Z. Meng, S. Zhang, Reusable and efficient polymer-supported task-specific ionic liquid catalyst for cycloaddition of epoxide with co2, Catal. Today 148 (3) (2009) 361–367.
[14] S. Ding, M. Radosz, Y. Shen, Ionic liquid catalyst for biphasic atom transfer radical polymerization of methyl methacrylate, Macromolecules 38 (14) (2005) 5921–5928.
[15] A. Berthod, M. Ruiz-Angel, S. Carda-Broch, Ionic liquids in separation techniques, J. Chromatogr. A 1184 (1) (2008) 6–18.
[16] A.B. Pereiro, J.M.M. Araujo, J.M.S.S. Esperanca, I.M. Marrucho, L.P.N. Rebelo, Ionic liquids in separations of azeotropic systems - a review, J. Chem. Thermodyn. 46 (2012) 2–28, https://doi.org/10.1016/j.jct.2011.05.026.
[17] K. Grygiel, L. Chabanne, Y. Men, J. Yuan, Thiazolium-containing poly(ionic liquid)s and ionic polymers, in: EUPOC 2013 Conference on Polymers and Ionic Liquids, Gargnano, Italy, Sep 01-05, 2013, Macromol. Symp. 342 (1, SI) (2014) 67–77, https://doi.org/10.1002/masy.201300171.
[18] D.W. Bruce, Y. Gao, J.N. Canongia Lopes, K. Shimizu, J.M. Slattery, Liquid-crystalline ionic liquids as ordered reaction media for the Diels-Alder reaction, Chemistry-A Eur. J. 22 (45) (2016) 16113–16123, https://doi.org/10.1002/chem.201602965.
[19] K.D. Clark, O. Nacham, J.A. Purslow, S.A. Pierson, J.L. Anderson, Magnetic ionic liquids in analytical chemistry: a review, Anal. Chim. Acta 934 (2016) 9–21, https://doi.org/10.1016/j.aca.2016.06.011.
[20] A. Abragam, The Principles of Nuclear Magnetism, Clarendon Press, Oxford, 1961.
[21] R. Kimmich, NMR - Tomography, Diffusometry, Relaxometry, Springer-Verlag, Berlin Heidelberg, 1997.
[22] R. Cordeiro, M.J. Beira, C. Cruz, J.L. Figueirinhas, M.C. Corvo, P.L. Almeida, A.A. Rosatella, C.A.M. Afonso, C.I. Daniel, P.J. Sebastião, Tuning the 1h nmr paramagnetic relaxation enhancement and local order of [aliquat]+-based systems mixed with dmso, Int. J. Mol. Sci. 22 (2) (2021), https://doi.org/10.3390/ijms22020706, https://www.mdpi.com/1422-0067/22/2/706.
[23] V. Overbeck, H. Schröder, A.-M. Bonsa, K. Neymeyr, R. Ludwig, Insights into the translational and rotational dynamics of cations and anions in protic ionic liquids by means of nmr fast-field-cycling relaxometry, Phys. Chem. Chem. Phys. 23 (2021) 2663–2675, https://doi.org/10.1039/D0CP05440B.
[24] F. Carniato, L. Tei, M. Botta, E. Ravera, M. Fragai, G. Parigi, C. Luchinat, 1h nmr relaxometric study of chitosan-based nanogels containing mono- and bis-hydrated gd(iii) chelates: clues for mri probes of improved sensitivity, ACS Appl. Bio Mater. 3 (12) (2020) 9065–9072, https://doi.org/10.1021/acsabm.0c01295.
[25] L.M. Brito, F.V. Chávez, M.I. Bruno Tavares, P.J. Sebastão, Analysis method, Polym. Test. 32 (7) (2013) 1181–1185, https://doi.org/10.1016/j.polymertesting.2013.07.002.
[26] M. Hofmann, B. Kresse, L. Heymann, A.F. Privalov, L. Willner, N. Fatkullin, N. Aksel, F. Fujara, E.A. Rössler, Dynamics of a paradigmatic linear polymer: a proton field-cycling nmr relaxometry study on poly(ethylene-propylene), Macromolecules 49 (22) (2016) 8622–8632, https://doi.org/10.1021/acs.macromol.6b01906.
[27] A. Aluculesei, H. Cachitas, J. Carvalho, F. Vaca Chavez, J.L. Figueirinhas, P.J. Sebastião, C. Cruz, M.G. Tamba, A. Kohlmeier, G.H. Mehl, 1h nmr study of molecular order and dynamics in the liquid crystal cb-c9-cb, Phys. Chem. Chem. Phys. 21 (2019) 4523–4537, https://doi.org/10.1039/C8CP06868B.
[28] D. Kruk, M. Wojciechowski, M. Florek-Wojciechowska, R.K. Singh, Dynamics of ionic liquids in confinement by means of nmr relaxometryexample, Materials 13 (19) (2020), https://doi.org/10.3390/ma13194351, https://www.mdpi.com/1996-1944/13/19/4351.
[29] A. Merbach, L. Helm, E. Toth (Eds.), The Chemistry of Contrast Agents in Medical Magnetic Resonance Imaging, 2nd edition, Wiley, 2013.
[30] D.J. Mastarone, V.S.R. Harrison, A.L. Eckermann, G. Parigi, C. Luchinat, T.J. Meade, A modular system for the synthesis of multiplexed magnetic resonance probes, J. Am. Chem. Soc. 133 (14) (2011) 5329–5337, https://doi.org/10.1021/ja1099616, pMID: 21413801.
[31] J. Kowalewski, P.H. Fries, D. Kruk, M. Odelius, A.V. Egorov, S. Krämer, H. Stork, M. Horvatić, C. Berthier, Field-dependant paramagnetic relaxation enhancement in solutions of Ni(II): what happens above the NMR proton frequency of 1 GHz?, J. Magn. Res. 314 (2020) 106737, https://doi.org/10.1016/j.jmr.2020.106737, https://www.sciencedirect.com/science/article/pii/S1090780720300550.
[32] A. Gradišek, T. Apih, M.J. Beira, C. Cruz, S.N. Fernandes, H.M. Godinho, P.J. Sebastião, Observing short-range orientational order in small-molecule liquids, Sci.

Rep. 12 (1) (2022) 22500, https://doi.org/10.1038/s41598-022-27187-7, https://europepmc.org/articles/PMC9797480.
[33] G.M.C. Silva, M.J. Beira, P. Morgado, L.C. Branco, P.J. Sebastião, J.N.C. Lopes, E.J.M. Filipe, Ionic liquids with hydrogenated and perfluorinated chains: structural study of the [p6, 6,6, 14][fncoo] n = 7, 9, 11. Checking the existence of polar – hydrogenated – perfluorinated triphilic continuity, J. Mol. Liq. (2022).
[34] R.E. Del Sesto, T.M. McCleskey, A.K. Burrell, G.A. Baker, J.D. Thompson, B.L. Scott, J.S. Wilkes, P. Williams, Structure and magnetic behavior of transition metal based ionic liquids, Chem. Commun. 4 (2008) 447–449, https://doi.org/10.1039/b711189d.
[35] P. Scovazzo, C.A. Portugal, A.A. Rosatella, C.A. Afonso, J.G. Crespo, Hydraulic pressures generated in magnetic ionic liquids by paramagnetic fluid/air interfaces inside of uniform tangential magnetic fields, J. Colloid Interface Sci. 428 (2014) 16–23, https://doi.org/10.1016/j.jcis.2014.04.023.
[36] M.D. Hanwell, D.E. Curtis, D.C. Lonie, T. Vandermeersch, E. Zurek, G.R. Hutchison, Avogadro: an advanced semantic chemical editor, visualization, and analysis platform, in: Avogadro: an Open-Source Molecular Builder and Visualization Tool, J. Cheminform. 4 (17) (2012), Version 1.2, http://avogadro.cc/.
[37] D. Van Der Spoel, E. Lindahl, B. Hess, G. Groenhof, A.E. Mark, H.J.C. Berendsen, Gromacs: fast, flexible, and free, J. Comput. Chem. 26 (16) (2005) 1701–1718, https://doi.org/10.1002/jcc.20291, https://onlinelibrary.wiley.com/doi/abs/10.1002/jcc.20291.
[38] K. Goloviznina, J.N. Canongia Lopes, M. Costa Gomes, A.A.H. Pádua, Transferable, polarizable force field for ionic liquids, J. Chem. Theory Comput. 15 (11) (2019) 5858–5871, https://doi.org/10.1021/acs.jctc.9b00689, pMID: 31525922, https://doi.org/10.1021/acs.jctc.9b00689.
[39] J.N. Canongia Lopes, A.A.H. Pádua, Molecular force field for ionic liquids III: imidazolium, pyridinium, and phosphonium cations; chloride, bromide, and dicyanamide anions, J. Phys. Chem. B 110 (39) (2006) 19586–19592, https://doi.org/10.1021/jp063901o, pMID: 17004824.
[40] C.E.S. Bernardes, Dlpgen: preparing molecular dynamics simulations with support for polarizable force fields, J. Chem. Inf. Model. 62 (6) (2022) 1471–1478, https://doi.org/10.1021/acs.jcim.1c01431.
[41] W. Humphrey, A. Dalke, K. Schulten, Vmd: visual molecular dynamics, J. Mol. Graph. 14 (1) (1996) 33–38, https://doi.org/10.1016/0263-7855(96)00018-5, https://www.sciencedirect.com/science/article/pii/0263785596000185.
[42] D. Sousa, G. Domingos Marques, J.M. Cascais, P.J. Sebastião, Desktop fast-field cycling nuclear magnetic resonance relaxometer, Solid State NMR 38 (1) (2010) 36–43.
[43] F. James, Minuit Function Minimization and Error Analysis, MINUIT Function Minimization and Error Analysis, 1994, Reference Manual Version 94.1.
[44] P.J. Sebastião, The art of model fitting to experimental results, Eur. J. Phys. 35 (1) (2014) 015017.
[45] P.J.O. Sebastiao, M.J. Beira, R.M.O. Cordeiro, A. Kumar, J.F. Fernandes, A.M.P. Ferraz, L.N. Gonçalves, The art of fitting ordinary differential equations models to experimental results, Eur. J. Phys. (2022), http://iopscience.iop.org/article/10.1088/1361-6404/ac563a.
[46] H.K. Kashyap, C.S. Santos, H.V.R. Annapureddy, N.S. Murthy, C.J. Margulis, E.W. Castner Jr, Temperature-dependent structure of ionic liquids: X-ray scattering and simulations, Faraday Discuss. 154 (2012) 133–143, https://doi.org/10.1039/C1FD00059D.
[47] K. Shimizu, M.F. Costa Gomes, A.A. Pádua, L.P. Rebelo, J.N. Canongia Lopes, Three commentaries on the nano-segregated structure of ionic liquids, in: Achievements and Challenges of Computational Chemistry in Portugal, J. Mol. Struct., Theochem 946 (1) (2010) 70–76, https://doi.org/10.1016/j.theochem.2009.11.034, https://www.sciencedirect.com/science/article/pii/S0166128009007684.
[48] Z. Khaknejad, N. Mehdipour, H. Eslami, Molecular dynamics simulation of the ionic liquid 1-n-butyl-3-methylimidazolium methylsulfate [bmim][meso4]: interfacial properties at the silica and vacuum interfaces, ChemPhysChem 21 (11) (2020) 1134–1145, https://doi.org/10.1002/cphc.202000197, https://chemistry-europe.onlinelibrary.wiley.com/doi/abs/10.1002/cphc.202000197.
[49] D.L. Mendivelso-Pérez, M.Q. Farooq, K. Santra, J.L. Anderson, J.W. Petrich, E.A. Smith, Diffusional dynamics of tetraalkylphosphonium ionic liquid films measured by fluorescence correlation spectroscopy, J. Phys. Chem. B 123 (23) (2019) 4943–4949, https://doi.org/10.1021/acs.jpcb.9b01476, pMID: 31095376.
[50] R. Dong, Nuclear Magnetic Resonance of Liquid Crystals, Springer, New York, 1997.
[51] R. Kimmich, Field-Cycling NMR Relaxometry: Instrumentation, Model Theories and Applications, The Royal Society of Chemistry, 2018.
[52] R. Kimmich, Field-Cycling NMR Relaxometry: Instrumentation, Model Theories and Applications, The Royal Society of Chemistry, 2018, Ch. 1.
[53] E. Belorizky, P.H. Fries, L. Helm, J. Kowalewski, D. Kruk, R.R. Sharp, P.-O. Westlund, Comparison of different methods for calculating the paramagnetic relaxation enhancement of nuclear spins as a function of the magnetic field, J. Chem. Phys. 128 (5) (2008) 052315, https://doi.org/10.1063/1.2833957, https://pubs.aip.org/aip/jcp/article-pdf/doi/10.1063/1.2833957/15407713/052315_1_online.pdf.
[54] A. Kasparek, A. Stankiewicz, M.J. Beira, P.J. Sebastião, R. Kruk, D. Kruk, 1h spin–lattice superparamagnetic relaxation enhancement over a wide range of magnetic fields-theory validation, J. Phys. Chem. B 129 (18) (2025) 4446–4453, https://doi.org/10.1021/acs.jpcb.5c00712, pMID: 40292482.
[55] J. Cho, J. Lee, Y. He, B. Kim, T. Lodge, C. Frisbie, High-capacitance ion gel gate dielectrics with faster polarization response times for organic thin film transistors, Adv. Mater. 20 (4) (2008) 686–690, https://doi.org/10.1002/adma.200701069, https://onlinelibrary.wiley.com/doi/abs/10.1002/adma.200701069.
[56] T. Kannan Kottummal, S. Pilathottathil, M.S. Thayyil, P. Mahadevan Perumal, K.K. Nagarajan Sreekala, G. Guruswamy, S. Vellikkandi Chaluvalappil, N.N. Manal Poovingal, Dielectric relaxation and electrochemical studies on trihexyl tetradecyl phosphonium chloride [p14, 6,6, 6][cl] ionic liquid, J. Mol. Liq. 252 (2018) 488–494, https://doi.org/10.1016/j.molliq.2017.12.146, https://www.sciencedirect.com/science/article/pii/S0167732217336590.
[57] E. Warburg, Ueber das verhalten sogenannter unpolarisirbarer elektroden gegen wechselstrom, Ann. Phys. 303 (3) (1899) 493–499, https://doi.org/10.1002/andp.18993030302, https://onlinelibrary.wiley.com/doi/abs/10.1002/andp.18993030302.
[58] M.E. Orazem, B. Ulgut, On the proper use of a Warburg impedance, J. Electrochem. Soc. 171 (4) (2024) 040526, https://doi.org/10.1149/1945-7111/ad3b76, https://dx.doi.org/10.1149/1945-7111/ad3b76.
[59] W. Bao, C. Fang, D. Cheng, Y. Zhang, B. Lu, D.H. Tan, R. Shimizu, B. Sreenarayanan, S. Bai, W. Li, M. Zhang, Y.S. Meng, Quantifying lithium loss in amorphous silicon thin-film anodes via titration-gas chromatography, Cell Rep. Phys. Sci. 2 (10) (2021) 100597, https://doi.org/10.1016/j.xcrp.2021.100597, https://www.sciencedirect.com/science/article/pii/S266638642100312X.
[60] S. Hori, R. Kanno, X. Sun, S. Song, M. Hirayama, B. Hauck, M. Dippon, S. Dierickx, E. Ivers-Tiffée, Understanding the impedance spectra of all-solid-state lithium battery cells with sulfide superionic conductors, J. Power Sources 556 (2023) 232450, https://doi.org/10.1016/j.jpowsour.2022.232450, https://www.sciencedirect.com/science/article/pii/S0378775322014276.